PCCP

Check for updates

Determination of helix orientations in a flexible DNA by multi-frequency EPR spectroscopy†

C. M. Grytz,‡[ab] S. Kazemi, [iD] ‡[bcd] A. Marko, [iD] [ab] P. Cekan, [e] P. Güntert, [iD] [bcfg]
S. Th. Sigurdsson [iD] *[e] and T. F. Prisner [iD] *[ab]

Distance measurements are performed between a pair of spin labels attached to nucleic acids using Pulsed Electron–Electron Double Resonance (PELDOR, also called DEER) spectroscopy which is a complementary tool to other structure determination methods in structural biology. The rigid spin label Ç, when incorporated pairwise into two helical parts of a nucleic acid molecule, allows the determination of both the mutual orientation and the distance between those labels, since Ç moves rigidly with the helix to which it is attached. We have developed a two-step protocol to investigate the conformational flexibility of flexible nucleic acid molecules by multi-frequency PELDOR. In the first step, a library with a broad collection of conformers, which are in agreement with topological constraints, NMR restraints and distances derived from PELDOR, was created. In the second step, a weighted structural ensemble of these conformers was chosen, such that it fits the multi-frequency PELDOR time traces of all doubly Ç-labelled samples simultaneously. This ensemble reflects the global structure and the conformational flexibility of the two-way DNA junction. We demonstrate this approach on a flexible bent DNA molecule, consisting of two short helical parts with a five adenine bulge at the center. The kink and twist motions between both helical parts were quantitatively determined and showed high flexibility, in agreement with a Förster Resonance Energy Transfer (FRET) study on a similar bent DNA motif. The approach presented here should be useful to describe the relative orientation of helical motifs and the conformational flexibility of nucleic acid structures, both alone and in complexes with proteins and other molecules.

[a] *Institute of Physical and Theoretical Chemistry, Goethe University, Max-von-Laue-Str. 7, 60438 Frankfurt am Main, Germany. E-mail: prisner@chemie.uni-frankfurt.de*
[b] *Center of Biomolecular Magnetic Resonance, Goethe University, Max-von-Laue-Str. 9, 60438 Frankfurt am Main, Germany*
[c] *Institute of Biophysical Chemistry, Goethe University, Max-von-Laue-Str. 9, 60438 Frankfurt am Main, Germany*
[d] *Frankfurt Institute for Advanced Studies, Ruth-Moufang-Str. 1, 60438 Frankfurt am Main, Germany*
[e] *University of Iceland, Department of Chemistry, Science Institute, Dunhaga 3, 107 Reykjavik, Iceland. E-mail: snorrisi@hi.is*
[f] *Laboratory of Physical Chemistry, ETH Zürich, Vladimir-Prelog-Weg 2, 8093 Zürich, Switzerland*
[g] *Graduate School of Science, Tokyo Metropolitan University, 1-1 Minami-osawa, Hachioji, Tokyo 192-0397, Japan*

† Electronic supplementary information (ESI) available: Optical melting studies, CW-EPR at the X-band, reproducibility of the modulation depth at the G-band, data analysis with respect to distance distributions, distance distribution predictions, details of the simulations and fits, predictions of high-field PELDOR data, fit to all experimental PELDOR data, fit with structures based on a geometric model, calculation of the helix axis and a movie illustrating the details of this structural ensemble for both representations. See DOI: 10.1039/c7cp04997h
‡ C. G. and S. K. contributed equally to this work.

Introduction

The structure and dynamics of nucleic acids play an important role in the determination of their biological functions, such as replication, transcription, and gene regulation.[1,2] Moreover, this knowledge can be important for a rational design of drugs.[3,4] Therefore, several biophysical techniques have been applied to study the structure and dynamics[5] of nucleic acids.

X-ray crystallography is classically used for the characterization of structures at atomic resolution. However, it requires crystals, which does not necessarily conserve the structure of their functional state. In addition, the conformational flexibility of highly flexible nucleic acid molecules cannot be accessed using this method. Nuclear Magnetic Resonance (NMR) spectroscopy allows elucidation of the secondary and compact tertiary structures as well as the dynamical behavior of nucleic acid molecules in solution with atomic resolution.[6,7] Residual dipolar couplings (RDCs) have been shown to yield orientational restraints between different segments of the nucleic acid structure using alignment media[8,9] or by paramagnetic spin labels or metal ions (paramagnetically induced residual dipolar couplings). In addition, spin labeling of oligosaccharides induces paramagnetic effects such as a pseudocontact shift[10] and paramagnetic

This journal is © the Owner Societies 2017

Phys. Chem. Chem. Phys., 2017, **19**, 29801–29811 | 29801

relaxation enhancement (PRE),[11,12] which offers other NOE-independent sources of long-distance information.[13] Dynamics can also be examined by relaxation dispersion experiments.[14,15] Flexibility can be characterized by "exact NOEs" in conjunction with structure calculations using ensemble-averaged distance restraints.[16] However, even using these NMR techniques, high quality structural data remain sparse for large, flexible nucleic acid molecules and their complexes due to resonance overlap, line broadening, and low proton density. Förster Resonance Energy Transfer (FRET) can detect long distances at a single molecule level at physiological temperatures by attaching two different fluorophore labels to the nucleic acid molecule. However, the size of the labels and their flexibility limit the accuracy of distance determination.[17,18]

Pulsed Electron–Electron Double Resonance (PELDOR),[19,20] also called DEER (Double Electron–Electron Resonance), spectroscopy has been used successfully to gain information on the structure and conformational flexibility of biomolecules on a nanometer scale (1.5–10 nm).[21–23] In such studies, the distance between two covalently attached spin labels is measured by determining the strength of the magnetic dipole–dipole coupling.[24] If rigid spin labels are incorporated into the biomolecule, the experimental PELDOR data will contain additional information about the mutual orientation of the two spin labels. This information can be extracted from sets of PELDOR time traces performed with varying probe frequencies and used as additional angular information for structure determination.[25] Moreover, rigid spin labels have no internal degrees of freedom and follow the motion of the biomolecule to which they are attached. Hence, the resulting distance distribution represents the conformational flexibility of the biomolecule itself. Since PELDOR data are recorded in frozen solutions, they reflect the conformational flexibility of the molecule at the freezing temperature. Therefore, the timescales of conformational transitions cannot be accessed by PELDOR, but the structural ensemble represents the overall flexibility of the molecule. This allows the determination of both the structure and the conformational flexibility of a biomolecule.[26–28] In contrast to the approach presented here, other PELDOR studies of DNA using flexible spin labels could not derive orientation information.[29–34]

In this work, we used the rigid nitroxide spin label Ç, a 2′-deoxycytidine-analogue,[35–37] which forms a Watson–Crick base pair with guanine (G) (Fig. 1A), thereby fixing its orientation within the DNA stem in which it resides.[38] Recently, we have shown that Ç enables the determination of the correlated twist–stretch motion of double-stranded DNA molecules.[39]

Here, we report the structure and conformational flexibility of a short double-stranded DNA molecule that contains a five-nucleotide bulge at the center (Fig. 1B). This bent DNA can be considered as a model for locally damaged DNA or more complex nucleic acids containing bulges, loops, junctions, and kinks. The structure and conformational flexibility of this DNA motif were previously investigated by NMR[40] and FRET[18] spectroscopy. Thus, it provides a good test case to evaluate the potential of PELDOR in conjunction with rigid spin labels. For molecules with a well-defined rigid structure, the signature of the corresponding
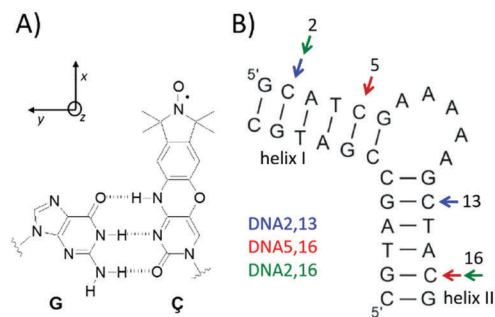
Fig. 1 (A) Spin label Ç, base-paired to guanine. (B) Secondary structure of the bent DNA and its three spin-labelled constructs **DNA2,13**, **DNA5,16** and **DNA2,16**. Arrows indicate labelling positions.

orientation-selective PELDOR dataset allows the unambiguous determination of the orientation between the two spin labels.[41] Due to the high flexibility of this DNA molecule, a single conformer alone cannot explain the experimental PELDOR data. In such cases, the situation is more complicated, since different structural bundles might represent the same orientation-selective PELDOR experiments equally well.[41] Therefore, we established a two-step protocol, in the literature classified as a sample and select method,[42,43] to derive a structural ensemble representing the flexibility of the DNA molecule.

In the first step, the boundaries derived from the PELDOR distance distributions and the published NMR data (NOEs and J-couplings) were applied to restrict the accessible conformational space of the two helices of this bent DNA. This first step delivers a library of topologically allowed structures of the DNA molecule. In the second step, the experimental orientation-selective PELDOR time traces were fitted using the conformers generated in the first step, resulting in a quantitative description of the conformational space of the DNA molecule. The uniqueness of the structural ensemble obtained from the PELDOR data at 0.3 T was checked by an independent PELDOR dataset recorded at high magnetic field strengths (6.2 T). Our results demonstrate that rigid spin labels can be used to determine structural ensembles of flexible nucleic acid molecules from a small number of doubly spin-labelled constructs.

Results and discussion

The DNA molecule, we investigated, has a bulge between its two helices, which induces a kink in the DNA structure (Fig. 1B). For the EPR experiments, one rigid Ç label was incorporated into each helix of the bent DNA. Three DNAs were prepared, each containing two labels: **DNA5,16** is labelled at C5 and C16, **DNA2,13** at positions C2 and C13, and **DNA2,16** at positions C2 and C16 (Fig. 1B). A decrease of the melting temperature by less than 3.5 °C, compared to the unmodified DNA, was observed for all DNA samples indicating that the spin label does not alter the base-pairing significantly. Further information regarding the melting studies (Table S1, ESI†) and continuous wave EPR measurements at room temperature (Fig. S1, ESI†) can be found in the ESI.†

PELDOR experiments

In order to obtain information on the distances and the relative orientations of the two Ç labels, orientation-selective PELDOR measurements were performed at different frequency bands/magnetic field strengths (Fig. S2 and S4, ESI†). Fig. 2A (X-band), Fig. S11 (Q-band) and Fig. S12 (G-band) (ESI†) show the results of these orientation-selective PELDOR measurements for the samples **DNA5,16**, **DNA2,13** and **DNA2,16**.

The PELDOR time traces oscillate with the characteristic frequency ν_{dip} of the dipole–dipole interaction between two nitroxide spin labels given by the formula:

$$\nu_{\mathrm{dip}}(R,\Theta) = \frac{52.16\,[\mathrm{MHz\,nm^3}]}{R^3}(3\cos^2\Theta - 1) \qquad (1)$$

where R is the spin–spin distance, and Θ is the angle between the dipolar vector $\vec{R}$ and the external magnetic field $\vec{B}_0$.

At X-band frequencies (9.6 GHz/0.3 T), the pump pulse, which is on-resonant with spins at the center of the nitroxide spectrum (Fig. S2, ESI†), excites all molecular orientations, whereas by the choice of the probe frequency, a well-defined sub-ensemble of nitroxide orientations with respect to the external magnetic field is selected. Since the X-band nitroxide spectrum is dominated by the anisotropic hyperfine interaction of the unpaired electron with the nitrogen nucleus, which has a large A_{zz} component, its orientation-selective PELDOR data provide information on the spin–spin distance and three angles (angle between the nitroxide out-of-plane normal, the A_{zz}-axis,

and the distance vector of each spin label, respectively and the angle between both A_{zz}-axes).[41] In contrast, the nitrogen hyperfine components A_{xx} and A_{yy} of the nitroxide spectrum are too small to be spectrally resolved and coincide with the central region of the spectrum excited by the pump pulse (Fig. S2, ESI†). This also implies a specific selection of Θ angles for different probe frequencies, if the relative orientation of the two helical parts of the DNA with respect to each other is not random. The weights of different dipolar axis orientations contributing to a PELDOR time trace with a specific probe frequency ν_A, depend on the angle Θ in a nontrivial way.[26] The separation of the dependencies on R and Θ in eqn (1) can be achieved by a quantitative analysis of the PELDOR time traces as a function of the probe frequency.[25]

Oscillation frequency, modulation depth and damping of the PELDOR signals change as a function of the selected probe frequency offset $\Delta\nu = \nu_A - \nu_B$, ranging from 40 to 90 MHz (Fig. 2A). This indicates that the relative orientation between the two Çs contributes to the shape of the PELDOR signal. The damping of the dipolar oscillations for **DNA5,16** increased as the frequency offset $\Delta\nu$ decreased from 90 to 40 MHz. The time traces of **DNA2,13** show the inverse effect. For **DNA2,16**, which is Ç-labelled close to the end of each helix, the PELDOR signals change weakly as a function of the probe frequency offset. Thus, the strongest orientation effect is observed for **DNA5,16**.

The distance distributions between two rigid spin labels were calculated by summing up all time traces recorded with different probe frequencies. By this procedure, the orientation correlations between the two spin labels are sufficiently averaged to obtain the distance distribution function by Tikhonov regularization in the same way as for flexible spin labels (Fig. 2B).[26,44] Further information on the PELDOR distance distribution calculation can be found in the ESI.† The mean distance and half width at half maximum obtained from the PELDOR data for all three doubly labelled DNA samples are: **DNA5,16**: 2.66 ± 0.26 nm, **DNA2,13**: 3.26 ± 0.26 nm and **DNA2,16**: 3.00 ± 0.45 nm. The relatively strong damping of the oscillations in the time traces and corresponding broad distance distributions indicate a high conformational flexibility of the DNA molecule. In the first step of our procedure, the minimum and maximum border values of these three distance distributions (indicated by dotted red lines in Fig. 2B) were used together with the NMR restraints from the literature[40] to generate the conformers, which were used in the second step of our procedure to describe the conformational flexibility of the DNA molecule.

The situation at Q-band frequencies (33.6 GHz/1.2 T) is different and more complicated (Fig. S2B, ESI†), since the anisotropies of the nitrogen hyperfine coupling and the g-tensor are of similar magnitude and interfere with each other to a large extent. The Q-band PELDOR time traces show negligible orientation selectivity (Fig. S11, ESI†). Therefore, we used the experimental Q-band results only as a control of the structural model obtained from the analysis of X-band PELDOR time traces, as explained later in the cross-validation section.
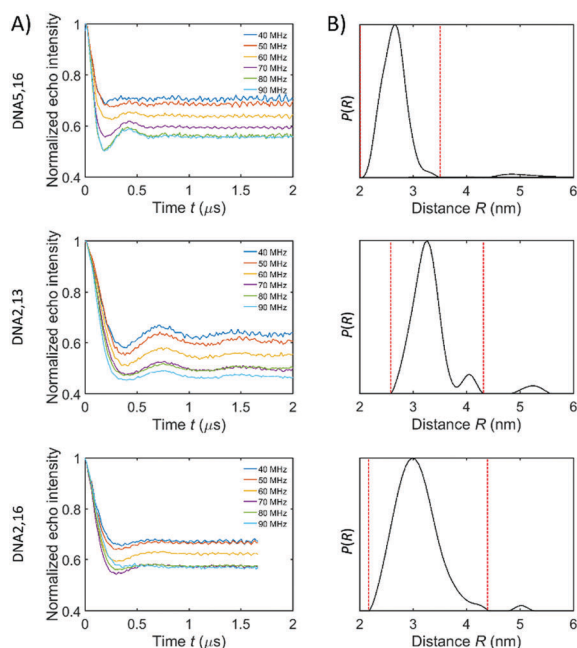
Fig. 2 (A) Experimental X-band PELDOR time traces for different frequency offsets $\Delta\nu$ between the probe and the pump frequency ranging from 40 to 90 MHz for **DNA5,16**, **DNA2,13** and **DNA2,16**. (B) Distance distributions based on a Tikhonov regularization of the X-band PELDOR data averaged over all measured frequency offsets $\Delta\nu$. The red dotted lines show the distance boundaries used in step 1 of our procedure for the selection of allowed conformers (*vide infra*).

This journal is © the Owner Societies 2017

Phys. Chem. Chem. Phys., 2017, **19**, 29801–29811 | **29803**

At G-band frequencies (180 GHz/6.4 T), all three principle values of the g-tensor are spectrally resolved, leading to nitroxide powder spectra with a width of about 250 G. This is much larger than the excitation bandwidth of the microwave pulses, which are approximately 5 G. Thus, the pump and probe pulses are both equally selective for specific orientations at G-band frequencies in contrast to PELDOR experiments performed at X-band frequencies. Therefore, the magnetic field positions were varied over the whole EPR spectrum. This procedure allows the determination of all five angles describing the orientation dependence of the dipolar interaction between two spin labels (three Euler angles that describe the relative orientation of the second nitroxide with respect to the first and two polar angles that describe the orientation of the dipolar vector with respect to the first nitroxide axis system).[41] Combined with the specific knowledge of the structure and the labelling scheme (3 spin labelled pairs), the inversion symmetry of the Spin Hamiltonian provides no additional ambiguities to the solutions. Consequently, the G-band PELDOR data depend strongly on the inter-helical orientations.

The orientation-selective measurements at G-band frequencies were performed on a home-built 180 GHz pulsed-EPR spectrometer[45,46] for the samples **DNA2,13** and **DNA2,16** (Fig. S12, ESI†). The PELDOR time traces were recorded by varying the external magnetic field with a constant frequency offset $\Delta\nu$ of 60 MHz (Fig. S2C and S12, ESI†). The modulation frequency, depth and damping of the PELDOR signals change depending on the pump and probe position in the EPR spectrum, which is a clear indication that the relative orientation between the two Çs contributes to the shape of the PELDOR signal. The most pronounced dipolar oscillation could be observed on a time trace recorded half way between the low field edge (g_{xx} position) and the maximum of the EPR spectra (g_{yy} position) for **DNA2,13** (position C in Fig. S2C and S12, ESI†). Dipolar modulations could be observed in all PELDOR time traces until reaching the high field edge (g_{zz} position). The experimental G-band data set was used as an independent and sensitive test of the conformational flexibility model obtained from the analysis of X-band PELDOR time traces. Moreover, the structural ensembles obtained from either fitting the X-band PELDOR data set alone or together with the G-band PELDOR time traces were analyzed and compared (Fig. S13D, ESI†).

The orientation-selective PELDOR data of the Ç-labelled DNA samples show orientation dependence, especially at X- and G-band frequencies. This complex pattern is a clear indication that the relative orientation contributes to the spectral shape and can in principle be used to extract angular information, in contrast to PELDOR experiments using flexible spin labels that only provide distance information.[47] The additional angular information of the rigid spin label used here strongly reduces the total number of spin-labelled samples that are required to provide an adequate number of structural restraints to describe the three-dimensional structure of a biomolecule. Moreover, the angular information is helpful in order to restrict the possible number of solutions for the overall structural ensemble that describes the conformational space of a flexible biomolecule.

Determination of the structural ensemble of the bent DNA

It is not always possible to extract all angular restraints in a straightforward manner from orientation-selective PELDOR data.[28,41] It is an ill-posed problem and hence different structural ensembles can represent the same orientation-selective PELDOR time traces. This is especially the case for flexible systems, if many conformers of the nucleic acid molecules coexist. Here, we use a two-step procedure (Fig. 3), which utilizes distance restraints from orientation-selective PELDOR data sets, NMR restraints (NOE and J-coupling) and topological constraints to select an ensemble of conformers for the bent DNA.

In the first step, we generated a large structure library of 15 000 structures by CYANA[48] containing a broad variety of conformations. There are examples of sampling of inter-helical Euler angles[49,50] or using molecular dynamics simulations[49,51] to generate such libraries. We used the PELDOR distance and NMR restraints.[34,52–56] In the case of a two-way junction, the long-distance PELDOR restraints between both helices are very helpful in restricting the conformational space describing the global arrangement of the helices relative to each other. Since the Ç spin labels are rigidly attached to the two helical parts of the molecule, the positions of the two unpaired electron spins can be easily calculated for all structures of the DNA molecule. For the PELDOR distance restraints, lower and upper bounds were manually set by inspection of the distance distribution functions (Fig. 2B red dotted lines). The distance for **DNA5,16**
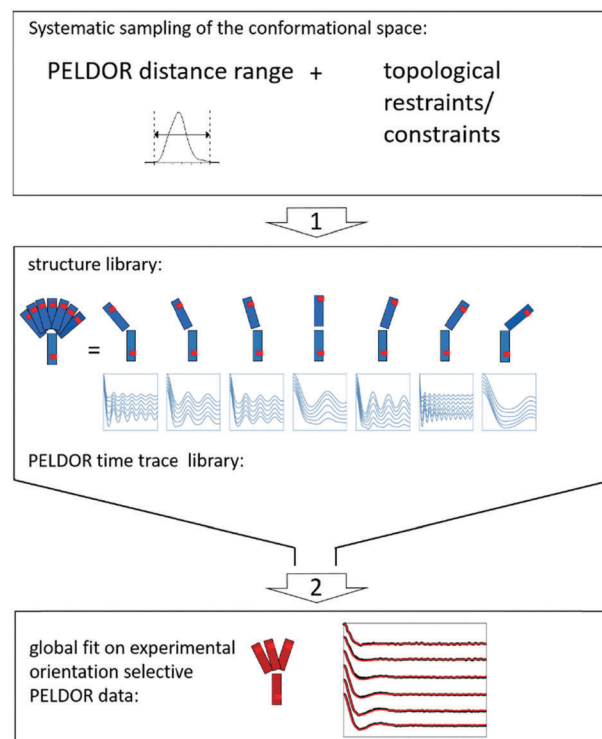
Fig. 3 Scheme of the structure determination protocol. In the first step, PELDOR distance information and restraints derived from NMR were used to create a structure library of conformers. In the second step, this library is used to fit the orientation-selective PELDOR data sets.

was restricted to 2.0–3.5 nm, for **DNA2,13** to 2.6–4.3 nm and for **DNA2,16** to 2.2–4.4 nm.

In the absence of other spectroscopic data, extraction of a structural ensemble from the orientation-selective PELDOR data can be done with PELDOR restraints and topological restrictions based on steric repulsion, as has been shown for the cocaine aptamer.[28] Since the structure of the bent DNA studied here had been investigated by NMR by Dornberger *et al.* using NMR spectroscopy (1QSK), a number of years ago,[40] we used both NOE and J-coupling data from that study as topological restraints. Whereas the ¹H NOEs and angular restraints from NMR are sufficient to describe the structure of the two helices, they only partially restrict the conformation of the bulge. Thus, the three distance restraints between the Ç spin pairs of the three DNA constructs were combined with the published NOE and J-coupling restraints.

The CYANA target function,[48] which measures how well the restraints are fulfilled, was used to filter out structures that were not in agreement with the spectroscopic data. The CYANA target function remained low despite the fact that the additional long-distance PELDOR restraints directed the conformational sampling towards structures of the bent DNA molecule, which were not favoured based on NMR restraints alone (Fig. S5, ESI†).[40] The CYANA target function does not increase significantly for distances within the chosen boundaries from PELDOR. Therefore, all the selected structures are in agreement with both the published NMR and the long-distance PELDOR restraints.

Next, the corresponding orientation-selective X-band PELDOR time traces were simulated for each structure of this restricted structure library. This yielded a library of PELDOR time traces in which each structure was represented by 18 time traces (3 labelling positions, 6 frequency offsets).

In the second step, the library of simulated time traces was used to fit the experimental data set. This was achieved by iteratively adding up the set of simulated time traces representing different conformers until satisfactory agreement with the experimental time traces set was obtained.[41] Since this fitting algorithm can select the same conformer several times, the statistical weight of each conformer within the ensemble is obtained immediately, as well as the relative spin label orientations and the distances.

The deviation between the sum of the selected simulated time trace set and the experimental time trace set decreased rapidly within a few iteration steps (Fig. S8, ESI†), resulting in an almost perfect fit to the experimental data. Fig. 4A shows that the ensemble of the structures obtained by this approach reproduces the experimental PELDOR time traces. In particular, the damping of the oscillations and its pattern is in very good agreement with the experimental time traces. Moreover, the distance distributions back-calculated from our structural ensemble are comparable in shape and mean distance to the distance distributions from the orientation-averaged time traces (Fig. S7, ESI†). This illustrates the internal consistency of our approach.

Characterization of the structural ensemble

Analysis of the experimental data gives a detailed picture of both the structure and the conformational flexibility of the bent DNA. The corresponding structural ensemble in which helix II

is overlaid in all structures is shown in Fig. 4B and C. The weights of the selected time traces correspond to the population of structures within the ensemble resulting in a statistical ensemble.[42] In this figure, the color saturation and transparency represent the population of the individual structures within the ensemble; the darker the color, the higher the population of a structure. Therefore, Fig. 4B and C give a description of the conformational flexibility of this DNA. The helices are shown as cuboids in Fig. 4B to visualize their relative orientation. An atomistic representation is shown in Fig. 4C. The conformational flexibility of the DNA molecule is characterized essentially by a broad continuum of conformers with a narrow region of higher population. A movie illustrating the details of this structural ensemble for both representations can be found in the ESI.†

The resulting structural ensemble and the conformational flexibility between the two helices, represented in Fig. 4B and C, can be characterized more quantitatively by their kink angle φ and twist angle θ (Fig. 5A). The kink angle is defined as the angle between the helix axes of each stem of the DNA.[42] The twist angle θ describes the rotation around the helix II axis. The calculation of the helix axis and of the helix angles can be found in the ESI.†

Fig. 5 shows density plots comparing the population of θ and φ pairs between the structure library created in step 1 (Fig. 5B) and the structures that were selected from the library in step 2 (Fig. 5C). The twist and kink angles for the structure library (Fig. 5B) are broadly distributed and show some correlation between them. This density plot clearly shows topological restrictions and topologically preferred inter-helical orientations dependent on both helix angles.[57] This was expected since the structure library was calculated based on PELDOR long distance ranges and repulsive van der Waals interactions.[57] The distribution of the φ angle in the structure library (Fig. 5B) shows a high density at positions that are different from those for the structures selected by the iterative fit procedure (Fig. 5C). Therefore, we conclude that the population distribution of the sampling has no influence on the selection of structures. In this density plot, we can compare our results to structure predictions obtained from the NMR data alone. The published NMR structures[40] are located in a highly populated region of the structural landscape derived in step 1 (Fig. 5B, black points). As expected, this indicates that the structural ensemble selected by CYANA in the first step based on the NMR and PELDOR distance restraints is in agreement with the published NMR structure bundle. Fitting of all experimental PELDOR time traces by a structural ensemble shifts the highest density of states to larger kink angles, as can be seen in Fig. 5C. This demonstrates the importance of the angular information encoded in the orientation-selective time traces, for the fitting procedure. Still, the published NMR structures with the third and the fourth lowest target function represent this region of highest density of conformational states. Thus, despite the fact that no PREs or RDCs were used in this NMR study[40] the most populated conformer obtained from the PELDOR data is still within the structural ensemble obtained by NMR. Only the conformational flexibility of the molecule was underestimated.

This journal is © the Owner Societies 2017

Phys. Chem. Chem. Phys., 2017, **19**, 29801–29811 | **29805**
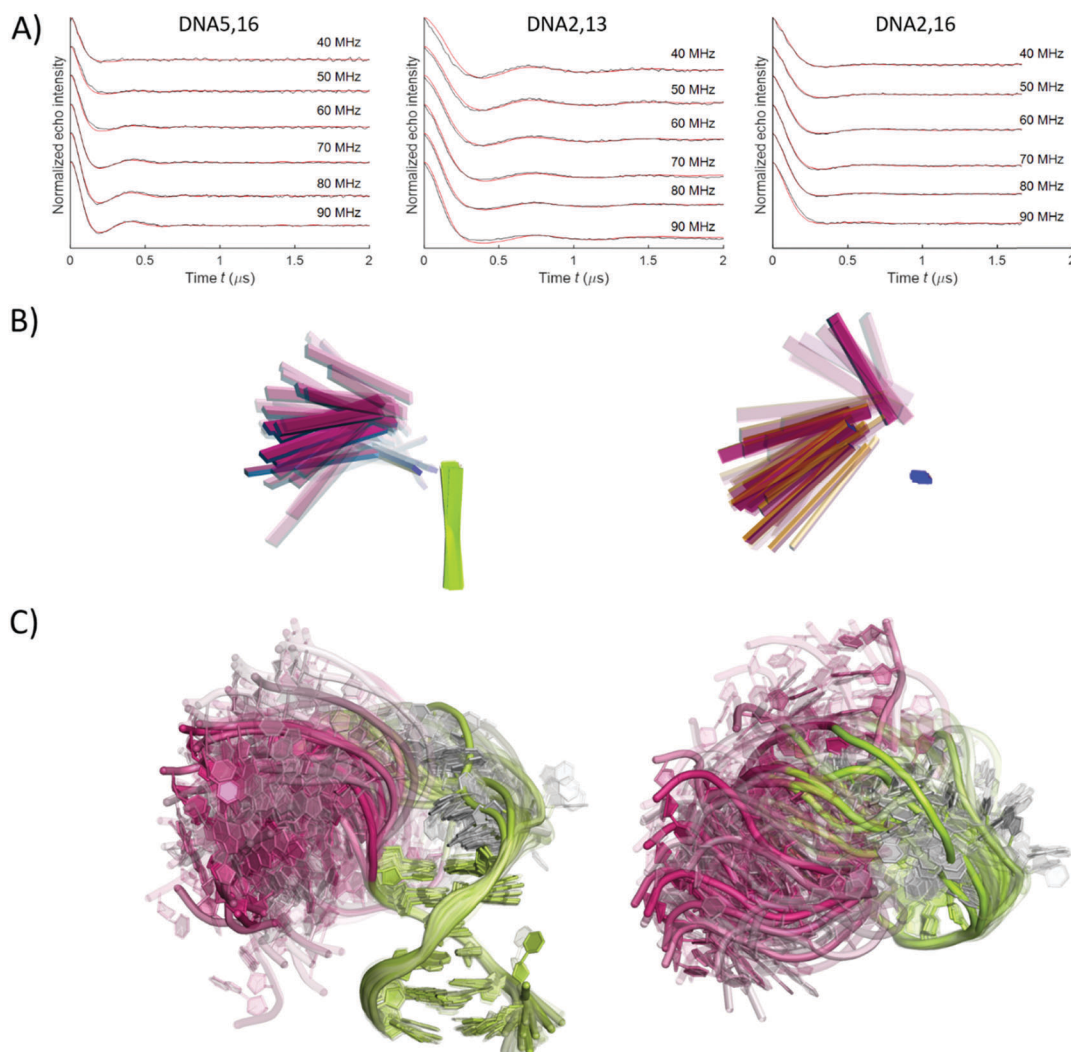
Fig. 4 (A) Comparison of experimental (black) and fitted (red) X-band PELDOR time traces for different frequency offsets $\Delta\nu$ for **DNA5,16**, **DNA2,13** and **DNA2,16**. Fitted PELDOR time traces were obtained by the two-step approach described in the text. The modulation depth of the PELDOR time traces (defined as the signal intensity at the end of the time trace at $t = 2.0$ µs) of the simulation has been adjusted to the experimental trace for better comparison. (B) Structural ensemble derived from this approach. The cuboids indicate the two helix axes. The structures were overlaid by helix II. The sides of the cuboids are differently colored to visualize the rotation of the helices relative to each other. The large opposed faces are colored in green, magenta, orange, and light blue, respectively. Both small faces of the cuboid are colored dark blue. The color saturation and percentage transparency represent the population of the individual structures within the ensemble. Views are shown from the side (left) where the magenta face and the green face of the cuboid representing helix I and helix II are visible, respectively. In the top view (right) the blue face of helix II and the orange and magenta faces of helix I are visible. (C) Atomistic model of the structural ensemble shown from the side and the top. The color saturation and percentage transparency represent the population of the individual structures within the ensemble. The structures were overlaid by helix II (helix II and the bulge are colored green; helix I is colored in magenta). A movie illustrating the details of this structural ensemble for both representations (see the ESI†).

For comparison, a library based on a simple geometric model without NMR data was generated. This library was used in the first step of the procedure to fit the PELDOR datasets. Although the resulting structural ensemble reproduces the PELDOR datasets reasonably (Fig. S9, ESI†) it probably contains non-native structures (Fig. 5B and Fig. S10, ESI†).

FRET has also been used to study a similar DNA containing five adenines in the bulge. While the most populated states of the FRET-based model[18] are also shifted to smaller kink angles, the width of the angular distribution obtained by the analysis of the FRET data agrees very well with our structural ensemble (Fig. 5C, green circles).[18] The absolute values of the twist angle

θ cannot be compared with the twist angle obtained by FRET since the base sequence is not the same for the DNA helices used in both studies (see the ESI† for details).

Solution NMR and FRET experiments are usually performed near room temperature, which is similar to physiological conditions for biomolecules. In contrast, PELDOR experiments have to be performed in the frozen state; on the one hand to slow down the fast electron spin relaxation and on the other hand to immobilize the molecules to avoid averaging of the dipolar coupling. Therefore, the timescale of conformational flexibility does not play a role for the interpretation of the PELDOR data, but can of course also not be determined.
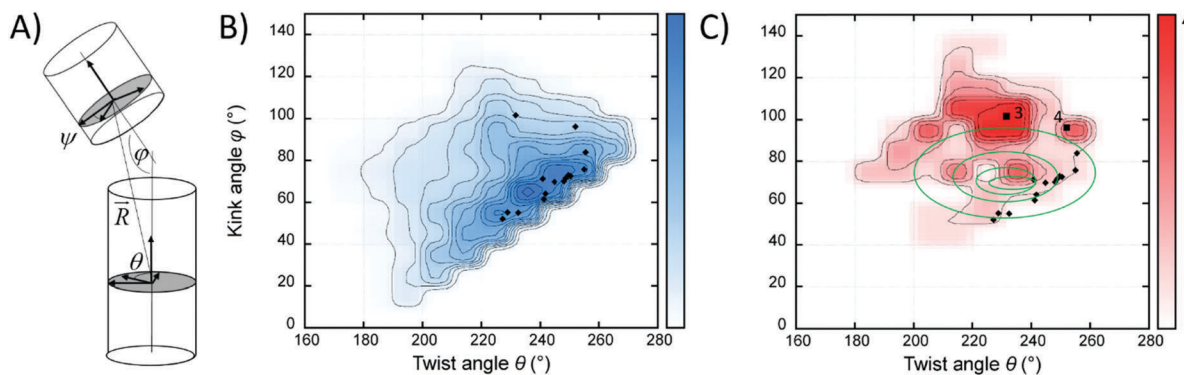
Fig. 5 (A) Definition of the kink φ and the twist angles ψ and θ. Both helices are represented as cylinders. (B) Density plot of θ against φ for all structures in the structure library (step 1). (C) Density plot of θ against φ for the structure ensemble selected out of the structure library in step 2 of the two-step approach. Each density plot has a resolution of 10° and the data points were smoothed by a Gaussian. Black points mark the structures from the published NMR structure bundle.[40] The structures with the third and the fourth lowest target function value of the published NMR structures are marked by 3 and 4, respectively. The height is normalized for both density plots separately. The green circles, which were extracted visually from Wozniak and coworkers,[18] represent the FRET structure bundle. The phase of the twist angle θ was chosen arbitrarily.

This differs from FRET, fluorescence and NMR experiments. However, freezing could be critical, because it might restrict the accessible conformational space of biomolecules.[58,59] In the case of double-stranded DNA, PELDOR data recorded at room temperature were shown to be in agreement with PELDOR data recorded at low temperatures.[33] The comparison of our results with the FRET data suggests that the conformational flexibility of the bent DNA molecule at room temperature is also well represented by the conformational distribution of the frozen sample (Fig. 5C). Our results reveal that the bent DNA molecule shows a broad conformational flexibility and exists in multiple conformational states that need to be considered for a quantitative simulation of the experimental PELDOR data.

Validation of the solution at X-band frequencies on high-field PELDOR data

As the A_{xx} and A_{yy} principle components of the hyperfine tensor are not spectrally resolved at X-band frequencies, only the kink angle between the two helices can be described by using X-band PELDOR data, whereas the twist angles of one helix relative to the other cannot be determined from only one spin label pair.[28] This is especially the case for flexible systems, where the solutions obtained from orientation-selective data of one Ç-labelled sample alone might not be unique. In the current study, the structures from the library were selected such that their corresponding simulated time traces agree simultaneously with all X-band time traces from the three different Ç-labelled samples. Even though a fit to the time traces of one spin label pair shows many possible solutions, an ensemble in agreement with the PELDOR data of all three DNA samples is expected to be much less ambiguous.

The consistency of the obtained structural ensemble can be tested in different ways. Here, the accuracy of the results was checked by a validation with orientation-selective measurements at higher magnetic fields where the x and y components of the anisotropic g-tensor are spectrally resolved. The resulting structural ensemble from the fit based on the experimental

X-band PELDOR data was used to directly predict high-field data recorded at Q- and G-band frequencies and compared to the corresponding experimental orientation-selective data. The structural ensemble reproduces the experimental G-band PELDOR data very well, except for the modulation depth (Fig. S12, ESI†). The discrepancy in the modulation depth was expected since the reproducibility of the modulation depth at this frequency band is rather poor due to experimental reasons (cavity Q-factor and coupling efficiency, see the ESI† and Fig. S3 for more details). Therefore, the modulation depth was neglected in the analysis of this data. Similarly, Q-band PELDOR time traces simulated from the structural ensemble based on restraints from X-band PELDOR data reproduced well the damping and the dipolar oscillation frequency (Fig. S11, ESI†).

To further test the robustness of our protocol, we used all the PELDOR time traces recorded at three magnetic field strengths for an overall fit. As shown in the ESI† (Fig. S13), the conformational spaces for the X-band fit and the multifrequency fit are comparable showing that the X-band data already comprise sufficient information to construct a meaningful structural ensemble.

Conclusion

In summary, we established a two-step protocol to investigate the conformational flexibility of DNA molecules. While there have been reports of using flexible spin labels to generate distance restraints to study proteins[52,53,60] and RNA[61] by a combination of PELDOR and NMR, we utilized rigid spin labels. This yielded angular information along with distance restraints. We have shown that distance and angular information from pulsed EPR using the rigid spin label Ç, along with topological restraints from NMR (NOE and J-coupling restraints) can be used to derive information about the global structure and conformational dynamics of a flexible two-way junction. This could be a general approach to investigate the structure and conformational dynamics of nucleic acid molecules. The lack of spin label

motion independent of the nucleic acid provides an opportunity to describe the conformational heterogeneity of nucleic acid molecules instead of static structures. This is urgently needed since many nucleic acids and their complexes with proteins or small molecules are dynamic in nature.[1,62] Since PELDOR has no limit on the size of the macromolecule, also larger DNA or RNA molecules (using Çm,[63,64] the RNA analog of Ç in conjunction with ligation techniques[23]) and their complexes with proteins and other molecules should be accessible by this methodology. This work lays the foundation for further studies to understand the global dynamics of nucleic acids at the atomic level and could provide essential knowledge for the mechanisms involved in DNA/RNA-protein recognition, which is important for many cellular processes.

Experimental

Sample preparation

The DNA molecule studied here consists of a 17-mer with the sequence 5′-d(GCATCGAAAAAGCTACG), which is paired with a 12-mer with the sequence 5′d(CGTAGCGATGC). The flexible 5-nucleotide bulge with the sequence dAAAAA (dA-bulge) (Fig. 1B) is located between two double-stranded regions. DNAs containing pairs of Ç spin labels (Fig. 1A) were synthesized as described previously by automated chemical synthesis, using the phosphoramidite derivative of Ç.[35,37] Sample preparations for the EPR experiments were very similar to the published NMR experiments[40] with respect to buffer conditions, DNA concentration, pH-value and metal ion concentration. After purification by denaturing polyacrylamide gel electrophoresis, 10 nmol of spin-labelled duplex DNA samples were annealed in 100 µl of 10 mM phosphate buffer (pH = 7), 100 mM NaCl and 0.1 mM EDTA, followed by evaporation of the solvent. Afterwards, they were dissolved in 100 µl of 20% ethylene glycol/water mixture. Ethylene glycol was used as a cryoprotectant.

PELDOR experiments

The dead-time-free 4-pulse ELDOR sequence[65] was used for all PELDOR experiments:

$$\pi/2(\nu_A) - \tau_1 - \pi(\nu_A) - (\tau_1 + t) - \pi(\nu_B) - (\tau_2 - t) - \pi(\nu_A)$$
$$- \tau_2 - \text{echo signal}$$

While NMR experiments were performed at room temperature, all PELDOR experiments were carried out in frozen aqueous buffer solution with a DNA duplex concentration of 100 µM at a temperature of 40 K.

Orientation-selective PELDOR experiments at X-band frequencies

Before the measurements all spin labelled samples with a volume of 100 µl were filled in EPR tubes (4 mm OD) and frozen in liquid nitrogen. Orientation-selective PELDOR experiments at X-band frequencies were performed for samples **DNA5,16**, **DNA2,13** and **DNA2,16** on a Bruker ELEXSYS E580 pulsed X-band EPR spectrometer. The spectrometer contains a standard

flex line probe head housing a dielectric ring resonator (MD5 W1) equipped with a continuous flow helium cryostat (CF935) and a temperature control system (ITC 502), both purchased from Oxford instruments. A commercially available setup (E580-400U) from Bruker was used to couple the second microwave frequency into the microwave bridge. All pulses were amplified via a pulsed travelling wave tube amplifier from Applied Systems Engineering (117X). The over-coupled resonator had a quality factor Q of about 100. The detection pulses ν_A were set to 32 ns for both π and $\pi/2$ pulses. The length of the pump pulse ν_B was 12 ns. The pump pulse was located at the maximum of the anisotropic powder spectrum selecting the nitrogen nuclear spin sublevel with $m_I = 0$ with random orientations of the nitroxide radical with respect to the external magnetic field (Fig. S2A, ESI†). This frequency was set at the resonance frequency of the resonator. The amplitude of the pump pulse was optimized by the inversion of a Hahn-echo at the frequency ν_B. The lengths of the detection pulses were chosen to minimize the overlap with the pump pulses. The frequency $\Delta\nu = \nu_A - \nu_B$ was varied from 40 to 90 MHz in steps of 10 MHz to select different orientations of the nitroxide radicals using the anisotropic nitrogen hyperfine tensor, as explained in the Results and discussion section. Therefore, the probe pulses were slightly off-resonance, but still within the bandwidth of the microwave resonator. Proton modulation was suppressed by the addition of 8 spectra with $\tau_1 = 136$, 144, 152, 160, 168, 176, 184, 192 ns. The time delay between the second and the third detection pulse ($\tau_1 + \tau_2$) was 2.5 µs. In order to eliminate receiver offsets, the $\pi/2$-pulse was phase-cycled (+0°, −180°). The video amplifier bandwidth was 50 MHz. The spectra for **DNA5,16** and **DNA2,16** were recorded with a repetition time of the pulse sequence of 4 ms. In the case of **DNA2,13** the repetition time was increased to 8 ms. Depending on the frequency offset $\Delta\nu$, the measurement time was about 2–3 h for $\Delta\nu = 40$–70 MHz and about 8–10 h for $\Delta\nu = 80$, 90 MHz.

PELDOR experiments at Q-band frequencies

All samples with a volume of 10 µl were filled in an EPR tube (1.6 mm OD) and fast frozen in liquid nitrogen before the measurement. The PELDOR experiments were performed at a temperature of 40 K, which was controlled using an Oxford continuous flow helium cryostat, on an ELEXSYS E580 spectrometer equipped with a Bruker ELEXSYS SuperQ-FT. A Bruker EN5107D2 resonator was used. The pulsed microwave power was 10 W, delivered from a solid state microwave amplifier (HA8019). The detection pulses ν_A were set to 48 ns for both π and $\pi/2$ flip angles. The frequency ν_A was 50 and 90 MHz higher than the resonance frequency of the microwave resonator. A length of 20 ns was chosen for the pump pulse with frequency ν_B, which was set on-resonance with the microwave cavity. The delay time τ_1 between the first and the second detection pulse was set to an initial value of 132 ns and incremented in 8 steps of 2 ns to reduce proton modulation. The pulse separation between the second and the third detection pulse ($\tau_1 + \tau_2$) was adjusted to 3 µs. 30 scans were accumulated giving an approximate measurement time of 4 h to achieve an optimal signal to noise ratio.

29808 | *Phys. Chem. Chem. Phys.*, 2017, **19**, 29801–29811

This journal is © the Owner Societies 2017

Orientation-selective experiments at G-band frequencies

Orientation-selective PELDOR experiments were performed for the samples **DNA2,13** and **DNA2,16** on a home-built pulsed-EPR spectrometer[45,46] extended for two-frequency irradiation and controlled by the Specman4EPR software program.[66] The operating frequency was 180 GHz (G-band) corresponding to a static magnetic field of 6.4 T. The magnet consists of two superconductive coils whereupon the main coil creates a static magnetic field between 0 and 7 T. The second superconductive coil has a range between ±0.08 T and is used to tune the magnetic field during an experiment. The microwave, with a power of approximately 60 mW, was coupled to a cylindrical resonator which operates in TE_{011} mode. The pump frequency was set at a constant offset $\Delta\nu$ of 60 MHz below or above (marked with * in Fig. S2C, ESI†) the detection frequency either to achieve a better signal-to-noise ratio (in the case of **DNA2,13**) or a more pronounced dipolar oscillation pattern (in the case of **DNA5,16**). The detection pulses were adjusted to approximately 45 and 75 ns for $\pi/2$ pulse and π pulses, respectively, and are tuned to the cavity resonance frequency to achieve maximum echo intensity. The length of the pump pulse was about 75 ns and optimized for a maximum modulation depth. 500 averages per point were applied to improve the signal-to-noise ratio. A time window of maximally 2.2 μs (τ_2) between the second and third pulse and a repetition time of 5 ms (due to the low temperature of 40 K) were employed. To avoid shifts of the microwave phase during the long accumulation time, the cryostat, probe head and the microwave bridge were thermally equilibrated for 1–2 h. To obtain the orientation dependent PELDOR time traces, the resonant field position was varied through the EPR powder spectrum (Fig. S2, ESI†). Time traces, consisting of around 60 to 120 scans, were recorded at several field values across the nitroxide EPR spectrum. The positions are marked by A, B... in Fig. S2C (ESI†).

Structure calculations

Structure calculations were performed using the program CYANA 3.9.[48,67] Previously, Dornberger *et al.* had solved the three-dimensional structure of this bent DNA (PDB ID: 1QSK) using restraints from 2D ^{1}H and ^{31}P NMR as well as IR and Raman spectroscopy.[40] 624 upper distance limits, 612 lower distance limits, and 235 torsion angle restraints from the original NMR data set for the structure determination were used. To include the EPR distance restraints into the structure calculations, the CYANA residue library was extended by an entry for Ç. A virtual atom (without any interaction with other atoms) placed at the center of the terminal N–O bond represents the unpaired electron and is used to define the PELDOR distance restraints between these virtual atoms. The spin label Ç was introduced into the DNA replacing the cytosines at the specific labeling positions C2, C5, C13, and C16. NMR restraints from the original NMR data referring to the replaced cytosines were applied to the corresponding atoms of Ç. Due to the lack of a corresponding hydrogen atom in Ç, restraints involving H5 of the replaced cytosines were discarded.

Protocol for ensemble determination

To generate a pool of structures (step 1 in Fig. 3) that broadly sample the conformational space of the bent DNA, we introduced distance restraints between the unpaired electrons of Ç5 and Ç16 (**DNA5,16**), Ç2 and Ç13 (**DNA2,13**), Ç2 and Ç16 (**DNA2,16**) in addition to the experimental NMR restraints. For these additional distance restraints, a 10 times higher weight than that for the NMR distance restraints was chosen. Structure calculations were performed for every distance restraint value combination by systematic variation of the target distances in the ranges of 20–35 Å, 26–43 Å and 22–44 Å for **DNA5,16**, **DNA2,13**, and **DNA2,16**, respectively, according to the corresponding PELDOR distance distributions (red lines in Fig. 2B). Within these ranges all three distances were varied systematically in steps of 0.5 Å with lower and upper distance bounds set at ±0.25 Å from the target distance of each distance restraint. For each distance combination 500 structures were calculated and the 20 conformers with the lowest CYANA target function were selected. The target function is defined as the sum of the squared deviations of the NMR restraints and the steric repulsion term, and the PELDOR distance restraints. To guarantee the agreement of the generated structures with the NMR data we selected only structures with a CYANA target function value below 4.0 Å^2. This cutoff was set below the maximum target function value found among the 20 best conformers obtained in a CYANA structure calculation using only the NMR data. In total, 14 254 of the structures that were calculated agreed with both, the PELDOR distance restraints and the NMR restraints. The fitting of the experimental PELDOR time traces in step 2 of our procedure was based on an iterative fitting algorithm developed in our group.[41] For each of the calculated N = 14 254 structures a corresponding PELDOR time trace set S_i was simulated (Fig. 3), resulting in a library S_{lib} of simulated PELDOR data sets.

$$S_{lib} = \{S_1,...,S_N\}$$

For each simulation, the pulse lengths, flip angles, magnetic field positions, and pump and probe frequencies were chosen according to the experiment. All equations necessary for PELDOR data simulation can be found in ref. 26, 41, 68 and 69. The g and hyperfine tensors are given in the ESI.†

An iterative fitting algorithm was applied to find an ensemble from the library of structures that optimally reproduce the experimental PELDOR data. In each iteration step n, the algorithm looks for the element $S_n \in S_{lib}$ that minimizes the error function Err_n, which is the difference between the experimental signal set S_{exp} and the sum of the simulated signal sets from the previous selection of signals $S_1,...,S_{n-1}$ plus S_n:

$$Err_n = \min_{S_n \in S_{lib}} \left(S_{exp} - \frac{1}{n} \sum_{i=1}^{n} S_i \right)^2 \qquad (2)$$

In all fittings described here, 100 iterative fitting steps (corresponding to an ensemble of 100 structures, with possible multiple occurrences of one structure) were performed.

Thereby, the resulting structural ensemble ensured a simultaneous fit to all experimental X-band PELDOR time traces. Additionally, all experimental time traces including Q- and G-band data were fitted for testing the robustness of the protocol. Modulation frequency, damping of the oscillations and modulation depth of the PELDOR time traces all depend on the relative orientation of the two spin labels. Because the modulation depth also depends on the microwave field strength, which is experimentally not so easy to reproduce exactly due to the resonator coupling and Q-factor, we allowed variation of the modulation depth of 5–10%, which is its error of reproducibility from experiment to experiment (at X-band frequencies if the experiments are performed under identical conditions).

Conflicts of interest

There are no conflicts to declare.

Acknowledgements

References

1 E. A. Dethoff, J. Chugh, A. M. Mustoe and H. M. Al-Hashimi, *Nature*, 2012, **482**, 322–330.

2 M. Fuxreiter, I. Simon and S. Bondos, *Trends Biochem. Sci.*, 2011, **36**, 415–423.

3 G. Bischoff and S. Hoffmann, *Curr. Med. Chem.*, 2002, **9**, 312–348.

4 O. Kennard and W. N. Hunter, *Angew. Chem., Int. Ed.*, 1991, **30**, 1254–1277.

5 L. Salmon, S. Yang and H. M. Al-Hashimi, *Annu. Rev. Phys. Chem.*, 2014, **65**, 293–316.

6 D. A. Torchia, *Prog. Nucl. Magn. Reson. Spectrosc.*, 2015, **84**, 14–32.

7 I. Bertini, K. S. McGreevy and G. Parigi, *NMR of Biomolecules: Towards Mechanistic Systems Biology*, Wiley-Blackwell, 2012.

8 M. Blackledge, *Prog. Nucl. Magn. Reson. Spectrosc.*, 2005, **46**, 23–61.

9 M. H. Bailor, C. Musselman, A. L. Hansen, K. Gulati, D. J. Patel and H. M. Al-Hashimi, *Nat. Protoc.*, 2007, **2**, 1536–1546.

10 C. Nitsche and G. Otting, *Prog. Nucl. Magn. Reson. Spectrosc.*, 2017, **98–99**, 20–49.

11 G. Otting, *Annu. Rev. Biophys. Biomol. Struct.*, 2010, **39**, 387–405.

12 G. M. Clore and J. Iwahara, *Chem. Rev.*, 2009, **109**, 4108–4139.

13 Y. Zhang, T. Yamaguchi and K. Kato, *Chem. Lett.*, 2013, **42**, 1455–1462.

14 M. Akke, *Curr. Opin. Struct. Biol.*, 2002, **12**, 642–647.

15 A. G. Palmer, C. D. Kroenke and J. P. Loria, *Methods Enzymol.*, 2001, **339**, 204–238.

16 B. Vögeli, S. Kazemi, P. Güntert and R. Riek, *Nat. Struct. Mol. Biol.*, 2012, **19**, 1053–1058.

17 T. Förster, *Ann. Phys.*, 1948, **2**, 55–75.

18 A. K. Woźniak, G. F. Schröder, H. Grubmüller, C. A. M. Seidel and F. Oesterhelt, *Proc. Natl. Acad. Sci. U. S. A.*, 2008, **105**, 18337–18342.

19 A. D. Milov, K. M. Salikhov and M. D. Shchirov, *Sov. Phys. Solid State*, 1981, **23**, 565–569.

20 A. D. Milov, A. B. Ponomarev and Y. D. Tsvetkov, *Chem. Phys. Lett.*, 1984, **110**, 67–72.

21 O. Schiemann and T. F. Prisner, *Q. Rev. Biophys.*, 2007, **40**, 1–53.

22 G. Jeschke, *Annu. Rev. Phys. Chem.*, 2012, **63**, 419–446.

23 P. Z. Qin and T. Dieckmann, *Curr. Opin. Struct. Biol.*, 2004, **14**, 350–359.

24 P. Nguyen and P. Z. Qin, *Wiley Interdiscip. Rev.: RNA*, 2012, **3**, 62–72.

25 O. Schiemann, P. Cekan, D. Margraf, T. F. Prisner and S. T. Sigurdsson, *Angew. Chem., Int. Ed.*, 2009, **48**, 3292–3295.

26 T. F. Prisner, A. Marko and S. T. Sigurdsson, *J. Magn. Reson.*, 2015, **252**, 187–193.

27 A. Marko, V. P. Denysenkov, D. Margraf, P. Cekan, O. Schiemann, S. T. Sigurdsson and T. F. Prisner, *J. Am. Chem. Soc.*, 2011, **133**, 13375–13379.

28 C. M. Grytz, A. Marko, P. Cekan, S. T. Sigurdsson and T. F. Prisner, *Phys. Chem. Chem. Phys.*, 2016, **18**, 2993–3002.

29 Q. Cai, A. K. Kusnetzow, W. L. Hubbell, I. S. Haworth, G. P. C. Gacho, N. Van Eps, K. Hideg, E. J. Chambers and P. Z. Qin, *Nucleic Acids Res.*, 2006, **34**, 4722–4730.

30 G. Sicoli, G. Mathis, S. Aci-Sèche, C. Saint-Pierre, Y. Boulard, D. Gasparutto and S. Gambarelli, *Nucleic Acids Res.*, 2009, **37**, 3165–3176.

31 N. A. Kuznetsov, A. D. Milov, V. V. Koval, R. I. Samoilova, Y. A. Grishin, D. G. Knorre, Y. D. Tsvetkov, O. S. Fedorova and S. A. Dzuba, *Phys. Chem. Chem. Phys.*, 2009, **11**, 6826–6832.

32 O. Schiemann, N. Piton, Y. G. Mu, G. Stock, J. W. Engels and T. F. Prisner, *J. Am. Chem. Soc.*, 2004, **126**, 5722–5729.

33 G. Y. Shevelev, O. A. Krumkacheva, A. A. Lomzov, A. A. Kuzhelev, O. Y. Rogozhnikova, D. V. Trukhin, T. I. Troitskaya, V. M. Tormyshev, M. V. Fedin, D. V. Pyshnyi and E. G. Bagryanskaya, *J. Am. Chem. Soc.*, 2014, **136**, 9874–9877.

34 O. Duss, M. Yulikov, G. Jeschke and F. H.-T. Allain, *Nat. Commun.*, 2014, **5**, 1–9.

35 N. Barhate, P. Cekan, A. P. Massey and S. T. Sigurdsson, *Angew. Chem., Int. Ed.*, 2007, **46**, 2655–2658.

36 P. Cekan and S. T. Sigurdsson, *Biochem. Biophys. Res. Commun.*, 2012, **420**, 656–661.

37 P. Cekan, A. L. Smith, N. Barhate, B. H. Robinson and S. T. Sigurdsson, *Nucleic Acids Res.*, 2008, **36**, 5946–5954.

38 T. E. Edwards, P. Cekan, G. W. Reginsson, S. A. Shelke, A. R. Ferre-D'Amare, O. Schiemann and S. T. Sigurdsson, *Nucleic Acids Res.*, 2011, **39**, 4419–4426.

39 A. Marko, V. Denysenkov, D. Margraf, P. Cekan, O. Schiemann, S. T. Sigurdsson and T. F. Prisner, *J. Am. Chem. Soc.*, 2011, **133**, 13375–13379.

40 U. Dornberger, A. Hillisch, F. A. Gollmick, H. Fritzsche and S. Diekmann, *Biochemistry*, 1999, **38**, 12860–12868.

41 A. Marko and T. F. Prisner, *Phys. Chem. Chem. Phys.*, 2013, **15**, 619–627.

42 M. Bonomi, G. T. Heller, C. Camilloni and M. Vendruscolo, *Curr. Opin. Struct. Biol.*, 2017, **42**, 106–116.

43 E. Ravera, L. Sgheri, G. Parigi and C. Luchinat, *Phys. Chem. Chem. Phys.*, 2016, **18**, 5686–5701.

44 A. Godt, M. Schulte, H. Zimmermann and G. Jeschke, *Angew. Chem., Int. Ed.*, 2006, **45**, 7560–7564.

45 M. M. Hertel, V. P. Denysenkov, M. Bennati and T. F. Prisner, *Magn. Reson. Chem.*, 2005, **43**, S248–S255.

46 V. P. Denysenkov, T. F. Prisner, J. Stubbe and M. Bennati, *Appl. Magn. Reson.*, 2005, **29**, 375–384.

47 R. Dastvan, E. M. Brouwer, D. Schuetz, O. Mirus, E. Schleiff and T. F. Prisner, *Biophys. J.*, 2016, **110**, 2195–2206.

48 P. Güntert, C. Mumenthaler and K. Wüthrich, *J. Mol. Biol.*, 1997, **273**, 283–298.

49 W. Andrałojć, E. Ravera, L. Salmon, G. Parigi, H. M. Al-Hashimi and C. Luchinat, *Phys. Chem. Chem. Phys.*, 2016, **18**, 5743–5752.

50 M. H. Bailor, A. M. Mustoe, C. L. Brooks and H. M. Al-Hashimi, *Nat. Protoc.*, 2011, **6**, 1536–1545.

51 L. Salmon, G. Bascom, I. Andricioaei and H. M. Al-Hashimi, *J. Am. Chem. Soc.*, 2013, **135**, 5457–5466.

52 Y. H. Yang, T. A. Ramelot, R. M. McCarrick, S. S. Ni, E. A. Feldmann, J. R. Cort, H. Wang, C. Ciccosanti, M. Jiang, H. Janjua, T. B. Acton, R. Xiao, J. K. Everett, G. T. Montelione and M. A. Kennedy, *J. Am. Chem. Soc.*, 2010, **132**, 11910–11913.

53 J. N. Rao, C. C. Jao, B. G. Hegde, R. Langen and T. S. Ulmer, *J. Am. Chem. Soc.*, 2010, **132**, 8657–8668.

54 S. J. Hirst, N. Alexander, H. S. Mchaourab and J. Meiler, *J. Struct. Biol.*, 2011, **173**, 506–514.

55 N. S. Alexander, R. A. Stein, H. A. Koteiche, K. W. Kaufmann, H. S. Mchaourab and J. Meiler, *PLoS One*, 2013, **8**, 14.

56 S. M. Islam, R. A. Stein, H. S. Mchaourab and B. Roux, *J. Phys. Chem. B*, 2013, **117**, 4740–4754.

57 M. H. Bailor, X. Sun and H. M. Al-Hashimi, *Science*, 2010, **327**, 202–206.

58 I. Krstić, O. Frolow, D. Sezer, B. Endeward, J. E. Weigand, B. Suess, J. W. Engels and T. F. Prisner, *J. Am. Chem. Soc.*, 2010, **132**, 1454–1455.

59 E. Duchardt-Ferner, J. E. Weigand, O. Ohlenschläger, S. R. Schmidtke, B. Suess and J. Wöhnert, *Angew. Chem., Int. Ed.*, 2010, **49**, 6216–6219.

60 S. Bibow, Y. Polyhach, C. Eichmann, C. N. Chi, J. Kowal, S. Albiez, R. A. McLeod, H. Stahlberg, G. Jeschke, P. Guntert and R. Riek, *Nat. Struct. Mol. Biol.*, 2017, **24**, 187–193.

61 O. Duss, E. Michel, M. Yulikov, M. Schubert, G. Jeschke and F. H. T. Allain, *Nature*, 2014, **509**, 588–592.

62 C. D. Mackereth and M. Sattler, *Curr. Opin. Struct. Biol.*, 2012, **22**, 287–296.

63 C. Hobartner, G. Sicoli, F. Wachowius, D. B. Gophane and S. T. Sigurdsson, *J. Org. Chem.*, 2012, **77**, 7749–7754.

64 I. Tkach, S. Pornsuwan, C. Hobartner, F. Wachowius, S. T. Sigurdsson, T. Y. Baranova, U. Diederichsen, G. Sicoli and M. Bennati, *Phys. Chem. Chem. Phys.*, 2013, **15**, 3433–3437.

65 R. E. Martin, M. Pannier, F. Diederich, V. Gramlich, M. Hubrich and H. W. Spiess, *Angew. Chem., Int. Ed.*, 1998, **37**, 2833–2837.

66 B. Epel, I. Gromov, S. Stoll, A. Schweiger and D. Goldfarb, *Concepts Magn. Reson.*, 2005, **26B**, 36–45.

67 P. Güntert and L. Buchner, *J. Biomol. NMR*, 2015, **62**, 453–471.

68 A. Marko, D. Margraf, H. Yu, Y. Mu, G. Stock and T. Prisner, *J. Chem. Phys.*, 2009, **130**, 064102.

69 B. Endeward, A. Marko, V. P. Denysenkov, S. T. Sigurdsson and T. F. Prisner, *Methods Enzymol.*, 2015, **564**, 403–425.

This journal is © the Owner Societies 2017

Phys. Chem. Chem. Phys., 2017, **19**, 29801–29811 | **29811**